Paper No.
C2020-14914

Investigations on the CO_2 Corrosion of Mild Steel in the Presence of Magnesium and Calcium Ions

Hamed Mansoori, David Young, Bruce Brown, Srdjan Nesic, Marc Singer
Institute for Corrosion and Multiphase Technology,
Department of Chemical & Biomolecular Engineering, Ohio University
342 West State Street
Athens, OH 45701
USA

ABSTRACT

Oilfield brine contains magnesium (Mg^{2+}) and calcium (Ca^{2+}) ions. Although carbon dioxide (CO_2) corrosion of mild steel and its corrosion products has been extensively studied, the effect of Mg^{2+} and Ca^{2+} are frequently overlooked by researchers. Usually, a simple test electrolyte with various percentages of dissolved sodium chloride (NaCl) has been employed to study the mechanism of CO_2 corrosion to avoiding complications relating to the water chemistry. The current paper is a continuation of a series of publications aimed at investigating the effect of water chemistries associated with Mg^{2+} and Ca^{2+} on the CO_2 corrosion mechanism. A combination of electrochemical methods, weight loss technique, and surface characterization tools were employed over the course of long-term experiments with a controlled water chemistry and well-defined mass transfer conditions. The presence of Ca^{2+} in the electrolyte and the formation of a uniform calcium carbonate ($CaCO_3$) layer on the steel surface facilitated precipitation of a protective iron carbonate ($FeCO_3$) adjacent to the substrate. Localized corrosion was observed in the presence of high concentration of Mg^{2+} but was not detected in the simultaneous presence of Ca^{2+} and Mg^{2+} with a typical concentration ratio observed in oilfields ($Ca^{2+}/Mg^{2+}=7$).

Key words: CO_2 corrosion, Mild steel, Magnesium, Calcium, Corrosion Product

INTRODUCTION

Brine coproduced with a hydrocarbon phase usually contains high concentrations of magnesium ions (Mg^{2+}) and calcium ions (Ca^{2+}). Indeed, such brines are typically saturated with respect to calcium carbonate ($CaCO_3$) and/or magnesium carbonate ($MgCO_3$), with varying concentrations depending on environmental and geologic conditions. Precipitation of carbonate scales will occur due to changes in operational parameters (e.g., pH, pCO_2, and temperature) when the fluid is transferred from the reservoir to surface facilities. It is worth mentioning that a pure $MgCO_3$ scale has rarely been observed in oilfields. Instead, when brine contains Mg^{2+} and Ca^{2+}, precipitation of a substitutional solid solution of calcium-magnesium carbonate ($Ca_xMg_{1-x}CO_3$) has been reported. This could be due to the fact that $MgCO_3$ precipitation kinetics is extremely slow compared to $CaCO_3$.[1–3] Therefore, when the system is thermodynamically supersaturated with respect to both of these carbonates, $CaCO_3$ nucleation and precipitation occur earlier. However, Mg^{2+} can incorporate into the lattice of $CaCO_3$ during the crystallization process because $MgCO_3$ (magnesite) and $CaCO_3$ (with which it shares a calcite-type structure) are isostructural.

Mechanisms of CO_2 corrosion of mild steel and the characteristics of its corrosion products (mainly $FeCO_3$ and Fe_3C) have been extensively studied, and documented.[4–8] However, most of these studies have been performed in various dilute solutions of sodium chloride (NaCl) while, in reality, Mg^{2+} and Ca^{2+} are also present in the brines produced from oil fields.[9] A recent review paper by the current authors has investigated the relevant literature and the existing gaps in understanding the effect of Mg^{2+} and Ca^{2+} on mild steel corrosion.[10] Mg^{2+} and Ca^{2+} are considered non-electroactive species, therefore, they do not directly participate in the electrochemical reactions involved in corrosion processes. However, they can alter the physiochemical properties of corrosion products and thus influence the corrosion mechanism. In a series of publications by the authors, the effect of Ca^{2+} and $CaCO_3$ scale on aqueous CO_2 corrosion of mild steel was studied for different scenarios in controlled water chemistry and well-defined mass transfer conditions.[11–13] The following conclusions can be drawn from the conducted experiments at different $CaCO_3$ saturation levels, [Ca^{2+}], ionic strength, and pH at 80°C, pCO_2 0.53 bar, in 1 wt.% NaCl aqueous solution, and with a 20-rpm impeller speed:

- The electrolyte's $CaCO_3$ saturation level, [Ca^{2+}], bulk pH, and temperature are crucial parameters in studying the effect of Ca^{2+} on CO_2 corrosion. Ignoring the influence of such parameter(s) is one of the main reasons for the existing discrepancies in the available literature on this topic.
- Fe_3C played a critical role in precipitation of $Fe_xCa_yCO_3$, x+y=1, and $FeCO_3$. The mole fraction of Ca in $Fe_xCa_yCO_3$ depended on [Ca^{2+}] in the bulk and the experimental conditions.
- The protective behavior of the surface layers was mainly due to the formation of $FeCO_3$ adjacent to the steel surface and not $Fe_xCa_yCO_3$ nor $CaCO_3$ scale. However, the presence of $Fe_xCa_yCO_3$ and/or $CaCO_3$ scale facilitated $FeCO_3$ precipitation and enhanced its protectiveness by acting as a mass transfer barrier of Fe^{2+} outwards from the steel and H^+ towards the steel.
- Although $CaCO_3$ is isostructural with $FeCO_3$, $CaCO_3$ scale was not protective against further corrosion where $FeCO_3$ was protective. Ca^{2+} comes from bulk solution while Fe^{2+} comes from the corroding steel surface. Therefore, $FeCO_3$ has superior adherence to steel. This makes $FeCO_3$ protective while $CaCO_3$ is not.
- No localized corrosion was observed in the presence of different concentrations of Ca^{2+} and uniformly formed $CaCO_3$ scale in the conducted experimental conditions. However, ununiformed precipitation of $CaCO_3$ scale along with change of water chemistry on the steel surface might lead to localized corrosion [14].

Now that a better understanding of the influence of Ca^{2+} on the CO_2 corrosion of mild steel has been achieved, it is relevant to first explore the individual effect of Mg^{2+} and then the effect of the simultaneous presence of Ca^{2+} and Mg^{2+} on corrosion of mild steel to simulate the oilfield brines. In the present study, the results related to two experimental scenarios are presented. In the first scenario, the electrolyte is saturated with respect to $MgCO_3$ with low and high [Mg^{2+}]. In the second scenario, the electrolyte is primarily saturated with respect to $CaCO_3$ and Mg^{2+} are introduced at a mass ratio Ca^{2+} over Mg^{2+} of 7 (a typical mass ratio observed in oilfields[9]). Precipitation kinetics of $CaCO_3$ is relatively fast and $CaCO_3$ was successfully precipitated on the substrate surface, as shown experimentally in a previous publication by the authors.[12] However, precipitation kinetics of $MgCO_3$ are very low and $MgCO_3$ did not precipitate in the laboratory environments, even from highly supersaturated solutions with respect to $MgCO_3$, as is described later on in this publication (cathodic polarization of the working electrode did not help, either). Therefore, unlike for the $CaCO_3$ scale, it proved impossible to precipitate and study the effect of solid $MgCO_3$ scale on CO_2 corrosion in the current experimental conditions. However, as mentioned earlier, a pure $MgCO_3$ scale is also rarely seen in oilfields.

The main objectives of this work are to:

- Investigate the effect of low and high concentrations of Mg^{2+} on the CO_2 corrosion mechanism of mild steel while the electrolyte is saturated with respect to $MgCO_3$ at applicable pH conditions (Scenario 1).
- Investigate the effect of the simultaneous presence of Mg^{2+} and Ca^{2+} (with $Ca^{2+}/Mg^{2+} = 7$, mass ratio) on the CO_2 corrosion mechanism of mild steel in a solution saturated with respect to $CaCO_3$ (Scenario 2).

Special efforts were made to control the water chemistry and flow characteristics in the experimental glass cell system, ensuring reproducibility and reliability of the data.

EXPERIMENTAL SETUP, TEST MATRICES, AND METHODOLOGY

Experimental Setup

The experimental setup is able to control [Fe^{2+}] and [H^+] by means of two independent ion-exchange resin loops (Na-form and H-form, respectively).[11] It should be mentioned that for experiments with lower pH value (5.5) and higher Mg^{2+} concentration (4,200 ppm), [Fe^{2+}] was not controlled due to the fact that the Na-form resin is unable to differentiate between Mg^{2+} and Fe^{2+} and takes up both dipositive cations. Therefore, after a short period, the resin becomes saturated with Mg^{2+} and Fe^{2+} and loses its effectiveness. Despite the inability to control [Fe^{2+}] at pH 5.5, the $FeCO_3$ saturation levels at pH 6.2 and 5.5 were still similar (due to the higher solubility of $FeCO_3$ at pH 5.5 as compared to pH 6.2). Therefore, the comparison of the results for both pH value is still valid. More detailed information about the Na-form and H-form ion-exchange resins are presented in a previous publication by the authors[11] and also in a paper by Zhonh, *et al.*[15] The experimental setup is equipped with an impeller to create uniform mass transfer across the specimens. It also includes stationary specimen holders, instead of the more conventional rotating cylinder electrode and hanging weight loss specimens, installed around a central impeller. Moreover, the design of specimen holders eliminate the risk of oxygen contamination during specimen retrieval from the test solution The flow characteristics of this experimental setup have been reported in a recent publication by the authors.[11]

Test Matrices

To address the first objective described earlier, $MgCO_3$-saturated experiments were conducted and repeated for two different bulk solution pH values, 6.2 and 5.5. Using different solution pH values permitted to use different dissolved Mg^{2+} concentrations while the solution was saturated with respect to $MgCO_3$. For each Mg^{2+}-containing experiment, a baseline experiment was performed, in an otherwise identical water chemistry condition. An $MgCl_2$ salt (ACROS Organics™) was used to prepare Mg^{2+}-containing solutions.

Table 1
Test matrix for experiments saturated with $MgCO_3$ at pH 6.2 and pH 5.5

Parameter	**Description**			
Material & Specimen Type	UNS G10180 with ferritic-pearlitic microstructure flat square specimen with 1.5 cm^2 exposed surface area			
Temperature	80°C			
pCO_2	0.53 bar			
pH	**6.2**		**5.5**	
Electrolyte	Baseline	Investigating effect of Mg^{2+} (low concentration)	Baseline	Investigating effect of Mg^{2+} (high concentration)
	1 wt.% NaCl +$NaHCO_3$ (Ionic Strength ≈0.18 M)	1 wt.% NaCl +$MgCl_2$ (Ionic Strength ≈0.18 M)	1 wt.% NaCl +$NaHCO_3$+ $NaClO_4$ (Ionic Strength ≈ 0.6 M)	1 wt.% NaCl +$MgCl_2$ (Ionic Strength ≈0.6 M)
[Mg^{2+}]	0	100 ppm	0	4,200 ppm
S_{MgCO_3}	0	1	0	1
S_{FeCO_3}	< 10			
Dissolved O_2	<5 ppb			
Reference Electrode	Saturated Ag/AgCl			
Impeller Rotation Speed	20 rpm			
Mass Transfer Conditions	Equivalent to 0.5 m/s in a 0.1m ID pipe			
Electrochemical Techniques	LPR, OCP, EIS			
Surface Analysis Techniques	XRD, SEM/EDS			
Test Duration	7 days			

The experimental conditions presented in Table **2** was employed to conduct experiments related to the second scenario when Mg^{2+} and Ca^{2+} are simultaneously present in the electrolytes. The solution was initially saturated with respect to $CaCO_3$ and undersaturated with respect to $MgCO_3$. An excess amount of granular $CaCO_3$, solid powder, was present at the beginning of the experiments to ensure that the solution remained saturated with respect to $CaCO_3$. Mg^{2+} was then added to the system using the $MgCl_2$ salt, targeting a mass ratio of Ca^{2+}/Mg^{2+} =7. In

the conducted experimental conditions, the [Ca^{2+}] was ~6000 ppm and the [Mg^{2+}] was ~857 ppm. Previous publications by the authors[11,12] provide more information about the preparation of the $CaCO_3$-saturated solution with excess $CaCO_3$ powder.

Table 2
Experimental condition to study the effect of simultaneous presence of [Mg^{2+}] and [Ca^{2+}] on CO_2 corrosion at pH 5.5

Parameter	**Description**	
Material & Specimen Type	UNS G10180 with ferritic-pearlitic microstructure flat square specimen with 1.5 cm^2 exposed surface area	
Temperature	80°C	
pCO_2	0.53 bar	
pH	5.5	
Electrolyte	Baseline	Ca^{2+}/Mg^{2+}=7 (mass ratio)
	1 wt.% NaCl + $NaHCO_3$ + $NaClO_4$ (Ionic Strength≈0.6 M)	0.85 wt.% NaCl + $CaCO_3$ + $MgCl_2$ (Ionic Strength≈0.6 M)
[Mg^{2+}]	0	857 ppm, $S_{MgCO_3 \approx 0.2}$
[Ca^{2+}]	0	6,000 ppm, $S_{CaCO_3 \approx 1}$
S_{FeCO_3}	< 10	
Dissolved O_2	< 5 ppb	
Reference Electrode	Saturated Ag/AgCl	
Impeller Rotation Speed	20 rpm	
Mass Transfer Conditions	Equivalent to 0.5 m/s in a 0.1m ID pipe	
Electrochemical Techniques	LPR, OCP, EIS	
Surface Analysis Techniques	XRD, SEM/EDS	
Experiment Duration	7 days	

Methodology

For each experiment, regardless of the scenarios, [Fe^{2+}] was measured twice daily by spectrophotometry using phenanthroline as the complexation reagent. The impeller rotational speed was set to 20 rpm, conferring a mass transfer rate similar to that encountered in a 0.1m ID pipe with a flow velocity of 0.5 m/s.[11] The specimens were made of UNS G10180 mild steel that has a ferritic-pearlitic microstructure. The electrochemical and weight loss specimens were wet-polished with silicon carbide abrasive papers up to 600 grit. Following the polishing process, the specimens were rinsed with isopropanol and placed in an ultrasonic cleaner for 2 minutes to remove any possible debris from the steel surface. Finally, they were dried by cold air and weighed prior to immersion into the test solutions. A three-electrode system, including working, counter, and reference electrodes, along with a Gamry Reference600™ potentiostat, was used

to conduct electrochemical measurements. The corrosion rate was measured at least twice daily using the linear polarization resistance (LPR) method. The open circuit potential (OCP) was also recorded. The duration of each experiment was 7 days. Two specimens were retrieved from the glass cell at days 2, 4, and 7 from each experiment to obtain the weight loss (WL) as well as to conduct surface characterization using techniques including scanning electron microscopy (SEM), energy dispersive X-ray spectroscopy (EDS), and X-ray diffraction (XRD).

The polarization resistance measurements obtained by LPR included determination of solution resistance. Electrochemical impedance spectroscopy (EIS) was used to measure the solution resistance and the polarization resistance at the metal/solution interface was consequently compensated.

In this study, a *B* value of 26 mV was used in the Stern-Geary equation to convert the experimental polarization resistance to a corrosion rate. This value is commonly accepted in CO_2 environments, but is not based on any specific Tafel slopes since the corrosion mechanism is not strictly charge transfer controlled. Instead, this *B* value was determined by best fit comparison between current densities and weight loss measurements.[16,17]

RESULTS AND DISCUSSION

In this section, the experimental results of the two scenarios are presented. First, results of experiments saturated with $MgCO_3$ conditions at two different pHs are discussed. Second, experimental results of the second scenario (simultaneous presence of $Ca^{2+}$and Mg^{2+}) are presented.

Scenario 1: Effect of $MgCO_3$-Saturated Solution at pH 6.2 & 5.5

Results and Discussion Related to the Experiments Conducted at pH 6.2

Figure 1 presents the comparison of corrosion rate (CR) by the LPR for $MgCO_3$-saturated experiments (Mg^{2+} *ca.* 100 ppm) and the baseline experiment, at pH 6.2. The error bars on the graphs provided in Figure 1, and other graphs throughout this paper, represent maximum and minimum values at each average point from two separate experiments. For each experiment, specimens at day 2, 4, and 7 were retrieved from the test solution to conduct weight loss and surface characterization (such specimens are indicated with gray squares in Figure 1).

Based on Figure 1, it seems that the presence of Mg^{2+} accelerated the CR in the active period compared to the baseline. However, after 4 days of exposure, the corrosion rate became similar for experiments with and without Mg^{2+}. At this time (pseudo-passivation), the corrosion product layers have fully developed and, as a result, the iron dissolution reaction (anodic reaction) is significantly retarded compared to the initial stage of the corrosion process (active corrosion period). The three corrosion periods indicated in Figure 1 are thoroughly explained in a previous publication.[11] In conclusion, the presence of Mg^{2+} at *ca.* 100 ppm did not alter the protectiveness of corrosion products when they are fully developed in the pseudo-passivation period. The only difference was the higher initial CR experienced in the solution saturated with $MgCO_3$ in the active corrosion period.

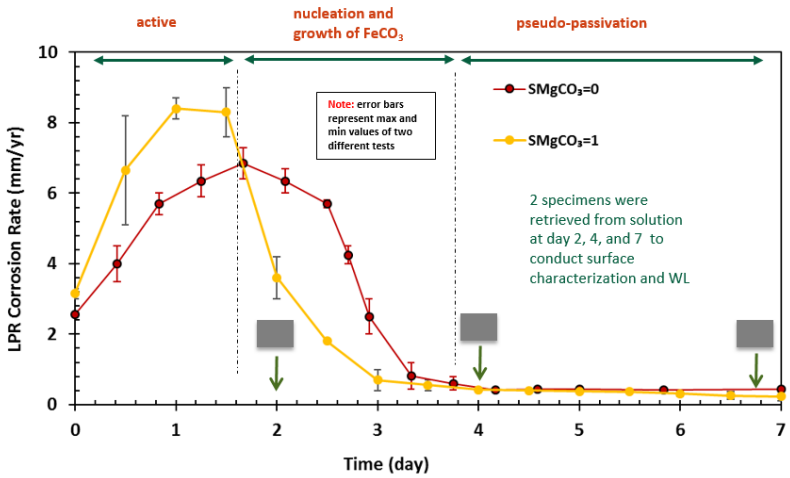

Figure 1: LPR corrosion rate over time with and without Mg^{2+} at pH 6.2

Specimens were retrieved from the test solutions on day 2, 4, and 7 of the experiments for surface layer characterization and measuring CR by the WL technique. Figure 2 shows a comparison of time-average CR by WL (bar chart) and LPR (line chart) at different exposure times for experiments with and without Mg^{2+}. Both LPR and WL methods show that CR decreases over time probably due to formation and development of corrosion product layers. Another observation is that although the initial CR in the presence of Mg^{2+} seems slightly higher than the baseline experiment (see CR by LPR in Figure 1), the cumulative CRs for both experiments are similar at the first two days; based on Figure 2. The thickness of the Fe_3C layer is also similar in both cases (see Figure 3). Fe_3C has been reported to act as an anchoring site for nucleation and crystal growth, collectively termed precipitation, of $FeCO_3$.[18,11]

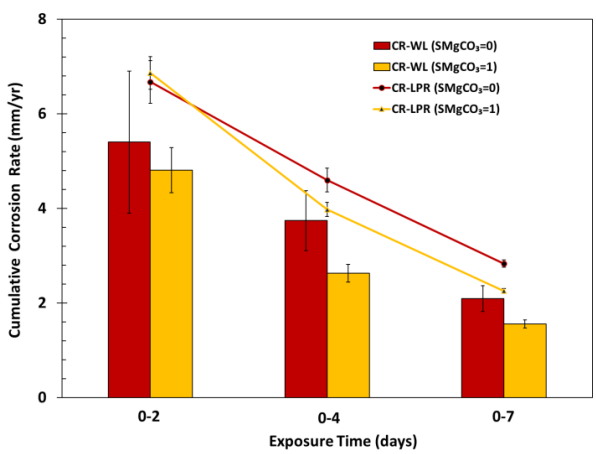

Figure 2: Cumulative corrosion rate by WL (bar chart) and LPR (line chart) techniques over time for solution with and without Mg^{2+} (80°C, pCO_2 0.53 bar, 0.5 m/s, pH 6.2, ionic strength 0.18 M, 1 wt/% NaCl)

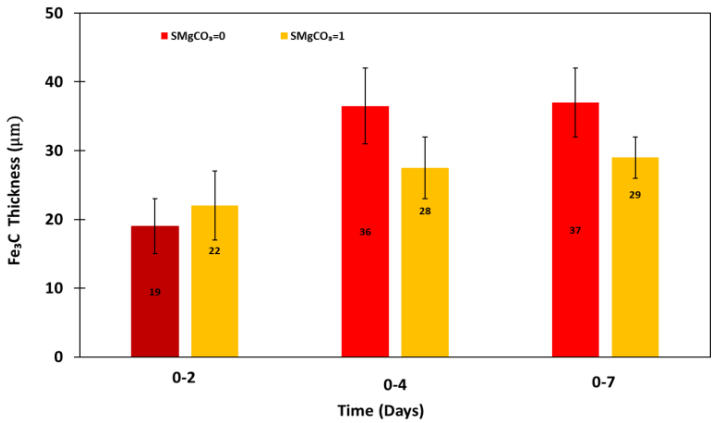

Figure 3: Evolution of Fe_3C over time with and without presence of Mg^{2+} (80°C, pCO_2 0.53 bar, 0.5 m/s, pH 6.2, ionic strength 0.18 M, 1 wt.% NaCl)

A comparison of open circuit potential (OCP) for experiments with and without Mg^{2+} is provided in Figure 4. The OCP trend with and without Mg^{2+} are identical with less negative OCP achieved at the end of both experiments (pseudo-passivation period) due to a better protectiveness offered by the corrosion products.

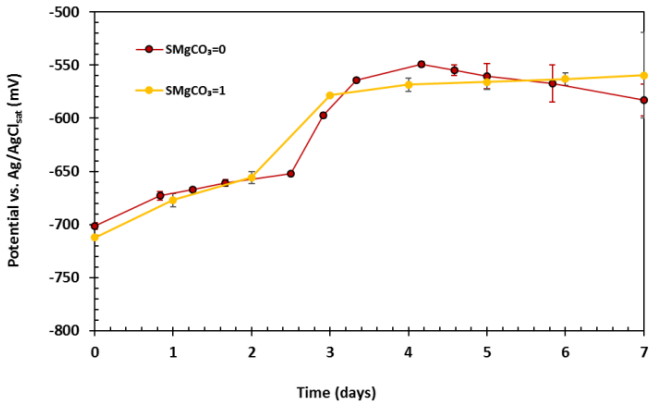

Figure 4: Comparison of OCP over time for UNS G10180 exposed to solutions with and without Mg^{2+} (80°C, pCO_2 0.53 bar, 0.5 m/s, pH 6.2, ionic strength 0.18 M, 1 wt.% NaCl)

Surface layers were characterized by SEM and the chemical compositional of the corrosion products and scales were analyzed by EDS. Furthermore, XRD was used to characterize the corrosion products on the steel surface.

SEM cross-sectional and top view images of surface layers developed without and with Mg^{2+} are provided in Figure 5 and Figure 6, respectively. The yellow arrows on the cross-sectioned specimens indicate the calculated metal loss depth based on WL corrosion rate. Such values were typically slightly greater than the measured corrosion product thickness. Overall, the morphology of surface layers is similar with and without the presence of Mg^{2+}. One difference is that the Fe_3C thickness in the presence of Mg^{2+} is higher in the first 2 days because of the higher corrosion rate. A greater thickness of Fe_3C means more favorable water chemistry for

precipitation of $FeCO_3$ within its pores. Upon precipitation of $FeCO_3$, CR would drop; Figure 1 is indicative of this phenomenon. A complete explanation for the role of Fe_3C in CO_2 corrosion over time is provided in a previous publication.[11,12]

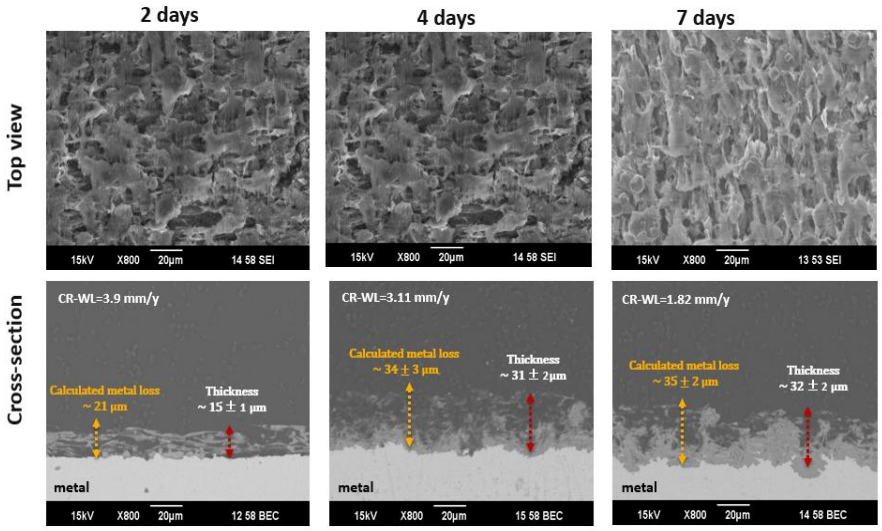

Figure 5: SEM images (top and cross-section view) of the development of surface layers over time for the experiment without presence Mg^{2+} ($S_{MgCO_3} = 0$) at 80°C, pCO_2 0.53 bar, 0.5 m/s, pH 6.2, ionic strength 0.18 M, 1 wt.% NaCl

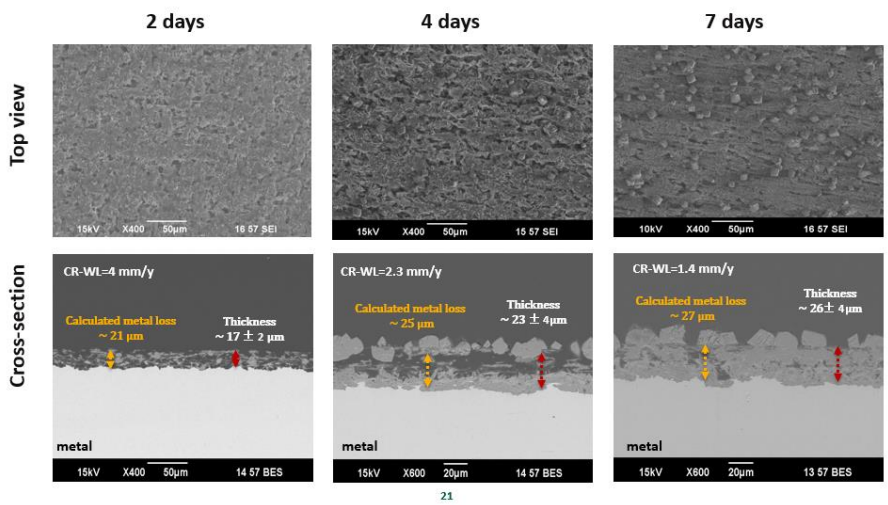

Figure 6: SEM images (top and cross-section view) of the development of surface layers over time for the experiment with presence of 100 ppm Mg^{2+} ($S_{MgCO_3} = 1$) at 80°C, pCO_2 0.53 bar, 0.5 m/s, pH 6.2, ionic strength 0.18 M, 1 wt.% NaCl

Figure 7 depicts a comparison of cross-sectional EDS line scan analysis of the surface layers developed on specimens exposed to solutions with and without Mg^{2+} after 7 days. $FeCO_3$ is the only corrosion product in the absence of Mg^{2+} (Figure 7 (a)). Even in the presence of Mg^{2+}, $FeCO_3$ was the only corrosion product existing adjacent to the steel surface. This inner layer was responsible for the final decrease in the corrosion rate (Figure 7 (b)). The formation of a

mixed iron-magnesium carbonate, as an outer layer, was confirmed by these analyses in the presence of Mg^{2+}. However, the mole fraction of Fe is significantly dominant over Mg in such a mixed metal carbonate.

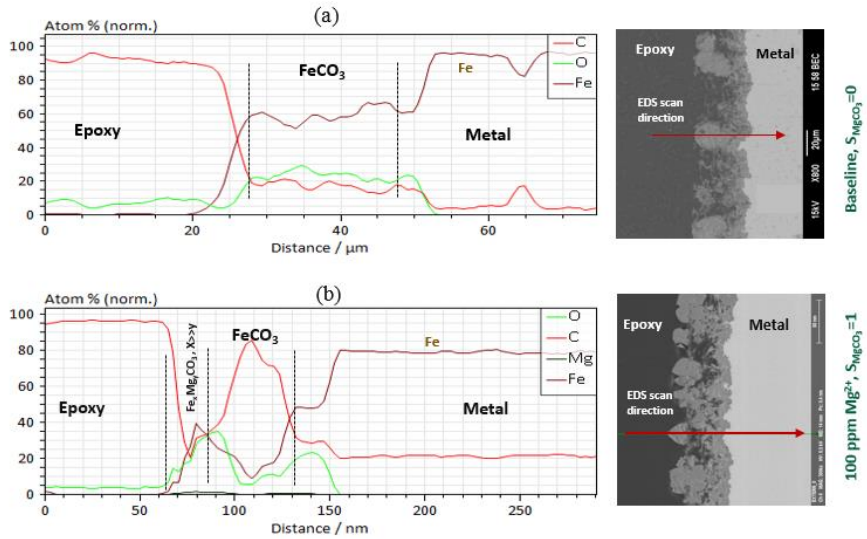

Figure 7: EDS line scan analysis of the surface layers developed on the specimens after 7 days of exposure to electrolytes without (a) and with (b) Mg^{2+} at 80°C, pCO_2 0.53 bar, 0.5 m/s, pH 6.2, ionic strength 0.18 M, 1 wt.% NaCl

Figure 8 shows the XRD data obtained for the specimens recovered from a $MgCO_3$-saturated solution with a Mg^{2+} concentration of *ca.* 100 ppm after 2 days (black line), 4 days (yellow line), and after 7 days (purple line) of exposure. XRD data shows that after 2 days of exposure, α-Fe and Fe_3C peaks are dominant over weak peaks related to $FeCO_3$. However, after 4 and 7 days of exposure, the intensity of peaks related to α-Fe and Fe_3C are noticeably diminished and, instead, peaks associated with $FeCO_3$ are intensified. The more intense peaks for $FeCO_3$ associated with (104) and (116) Miller planes located at 32.07 and 52.7 degrees 2θ (CuK_α radiation) are more easily recognizable after 4 and 7 days of exposure. However, $FeCO_3$ peaks are now broadened and shifted slightly towards the $MgCO_3$ reference peaks (green lines) after longer exposure time. Nevertheless, the incorporation of Mg^{2+} into the lattice of $FeCO_3$ was very limited compared to the similar condition with the presence of Ca^{2+}.[11]

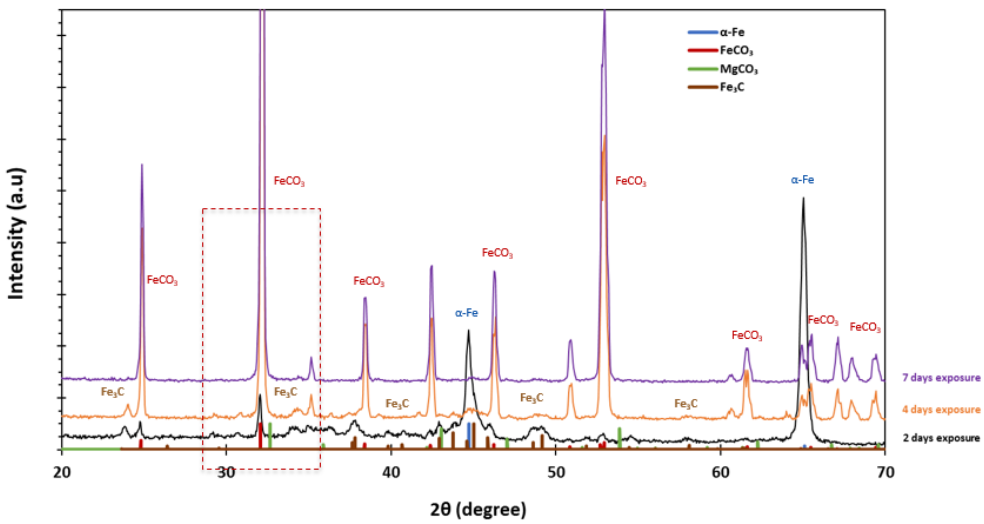

Figure 8: XRD patterns of surface layers detected on the steel surface after 2, 4, and 7 days of exposure to an electrolyte saturated with $MgCO_3$ at 80°C, pCO_2 0.53 bar, 0.5 m/s, pH 6.2, ionic strength 0.18 M, 1 wt.% NaCl

The susceptibility of the specimens to localized corrosion when exposed to solution with and without Mg^{2+} was also evaluated. Profilometry of the specimen surfaces was performed after removing corrosion product layers by Clarke solution [19]. No localized corrosion was observed for experiments conducted at bulk pH 6.2 with *ca.* 100 ppm Mg^{2+}. Figure 9 illustrates an example of profilometry of a specimen exposed for 7 days to a solution saturated with respect to $MgCO_3$.

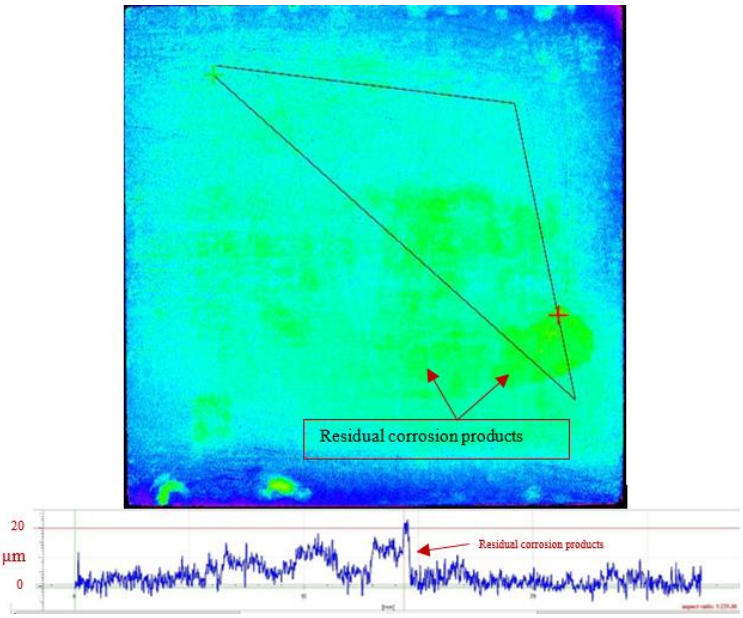

Figure 9: Example of profilometry of the specimen after removing the corrosion products (7 days of exposure to solution saturated with $MgCO_3$ at pH 6.2, 80°C, pCO_2 0.53 bar, ionic strength 0.18 M, 1 wt.% NaCl, Mg^{2+} ~ 100 ppm

Results and Discussion Related to the Experiments Conducted at pH 5.5

An additional experiment was conducted in similar conditions but at a higher concentration of Mg^{2+}, while the solution was still saturated with $MgCO_3$, to better resemble oilfield conditions. The experiment was conducted with 4,200 ppm Mg^{2+} at pH 5.5 (Table 2). Figure 10 shows the trend of LPR corrosion rate over time with and without Mg^{2+}. The three corrosion periods (active corrosion, nucleation/growth, pseudo-passivation) are identified similarly to the experiments conducted at pH 6.2. The final corrosion rates are higher compared to pH 6.2 because of the more aggressive solution (lower pH). Figure 11 shows cumulative corrosion rate with and without Mg^{2+}. According to WL results, the presence of 4,200 ppm Mg^{2+} leads to a higher average CR, especially after the first two days of exposure. This is reflected in the higher Fe_3C thickness as shown in Figure 12. The difference in CR becomes less pronounced as exposure time increases. The OCP variation over time for experiments conducted at pH 5.5 is shown in Figure 13.

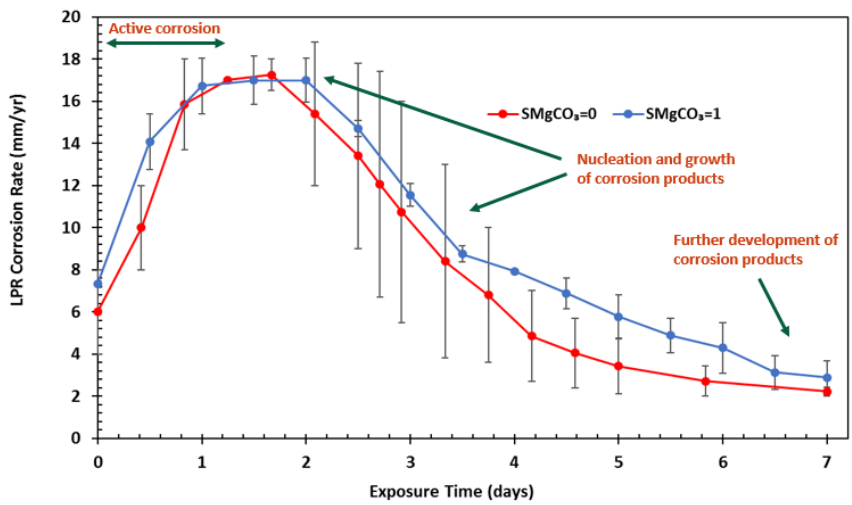

Figure 10: Trend of corrosion rate obtained by LPR over time with and without presence of Mg^{2+} at pH 5.5

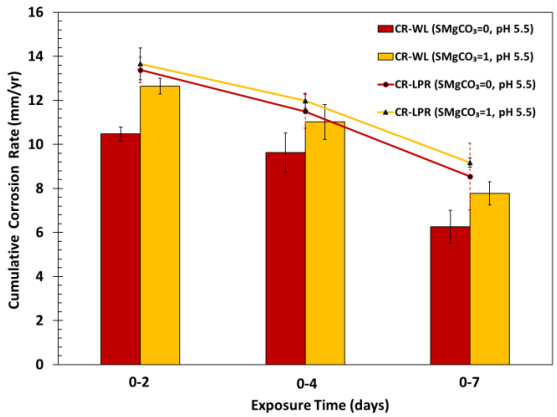

Figure 11: Cumulative corrosion rate by WL (bar chart) and LPR (line chart) techniques over time for solution with and without Mg^{2+} (80°C, pCO_2 0.53 bar, 0.5 m/s, pH 5.5, ionic strength 0.6 M, 1 wt.% NaCl)

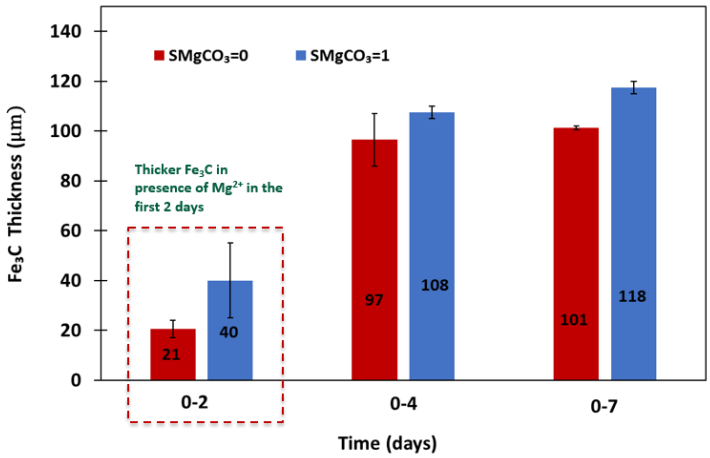

Figure 12: Evolution of Fe_3C over time with and without presence of Mg^{2+} (80°C, pCO_2 0.53 bar, 0.5 m/s, pH 5.5, ionic strength 0.6 M, 1 wt.% NaCl)

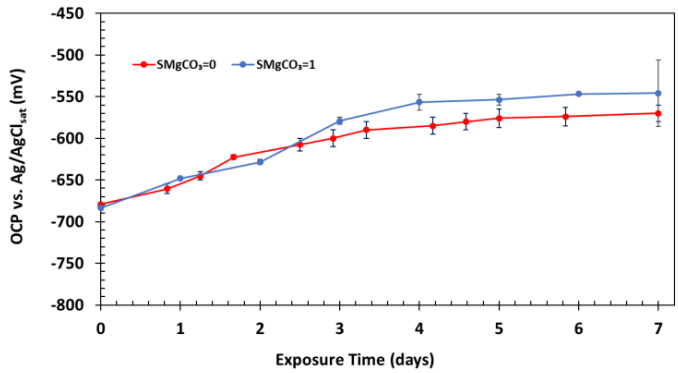

Figure 13: Comparison of OCP over time for UNS G10180 exposed to solutions with and without Mg^{2+} (80°C, pCO_2 0.53 bar, 0.5 m/s, pH 5.5, ionic strength 0.68 M, 1 wt.% NaCl)

SEM cross-sectional and top view images of surface layers developed without and with the presence of Mg^{2+} are shown in Figure 14 and Figure 15, respectively. The morphology and composition of corrosion products were similar to those obtained at pH 6.2 with lower [Mg^{2+}]. A greater thickness of corrosion products was achieved for experiments at pH 5.5 due to the higher corrosion rate.

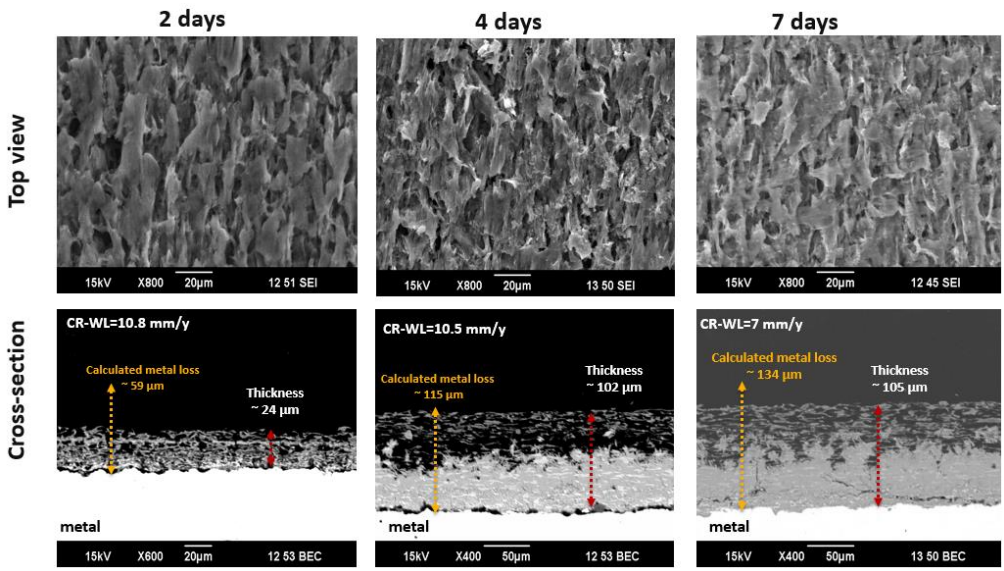

Figure 14: SEM images (top and cross-section view) of the development of surface layers over time for the experiment without presence of Mg^{2+} ($S_{MgCO_3} = 0$) at 80°C, pCO_2 0.53 bar, 0.5 m/s, pH 5.5, ionic strength 0.6 M, 1 wt.% NaCl

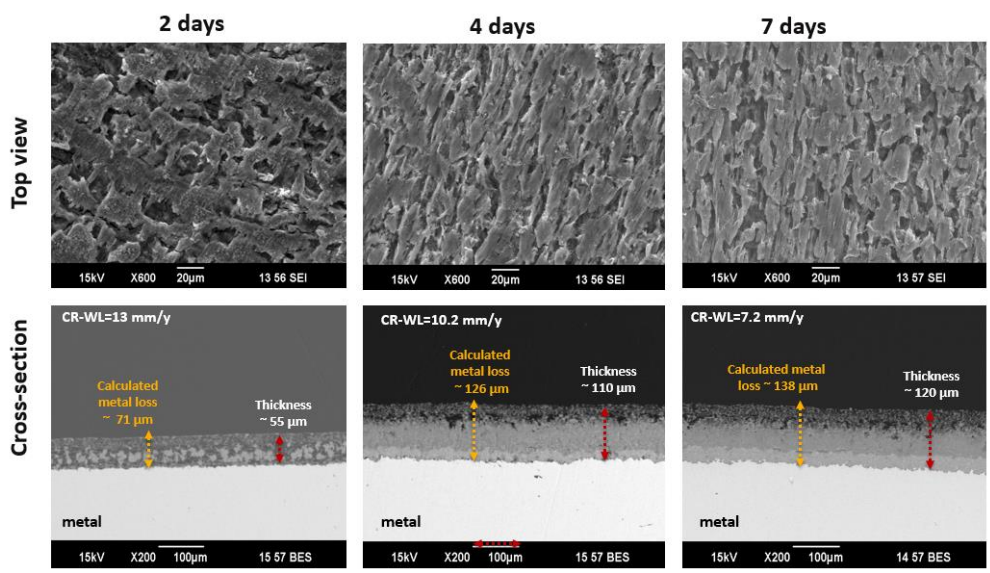

Figure 15: SEM images (top and cross-section view) of the development of surface layers over time for the experiment with presence of 4,200 ppm Mg^{2+} ($S_{MgCO_3} = 1$) at 80°C, pCO_2 0.53 bar, 0.5 m/s, pH 5.5, ionic strength 0.6M, 1 wt.% NaCl

Figure 16 shows a comparison of cross-sectional EDS line scan analysis of the surface layers developed on specimens exposed to solutions with and without 4,200 ppm Mg^{2+} after 7 days. $FeCO_3$ is the only corrosion product in the absence of Mg^{2+} (see Figure 16 (a)). Figure 7 (b), considering 4,200 ppm of Mg^{2+}, shows no significant Mg^{2+} incorporation into the lattice of $FeCO_3$. Likewise, for the experiment with lower [Mg^{2+}], a solid solution of $Fe_xMg_yCO_3$ formed on the steel surface with x>>y. Formation of a bi-layer of corrosion product on the specimen is confirmed from Figure 7 (b).

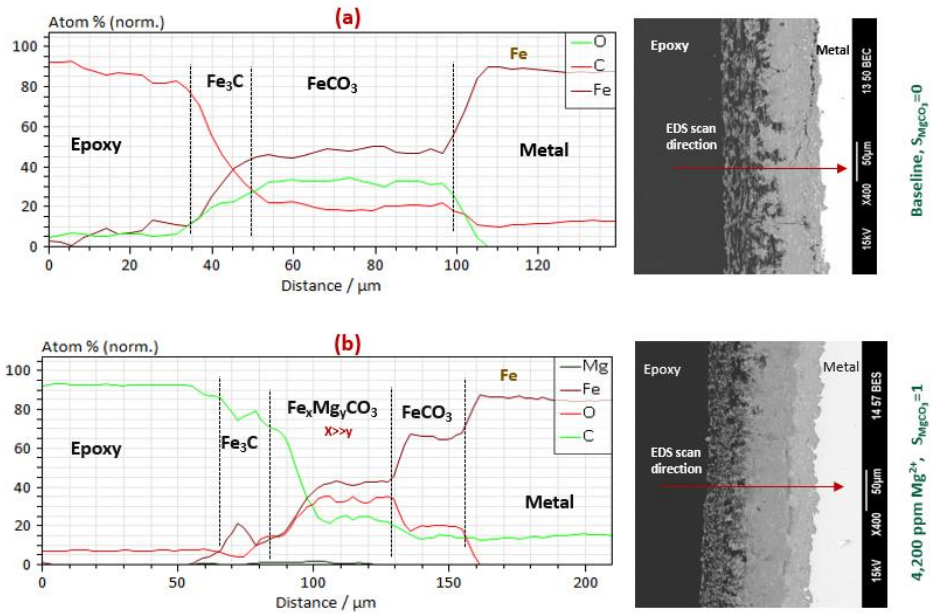

Figure 16: EDS line scan analysis of the surface layers developed on the specimens after 7 days of exposure to electrolytes without (a) and with (b) 4,200 ppm Mg^{2+} at 80°C, pCO_2 0.53 bar, 0.5 m/s, pH 5.5, ionic strength 0.6M, 1 wt.% NaCl

Unlike the experiments conducted at low [Mg^{2+}], localized corrosion was observed with high [Mg^{2+}] at the lower pH of 5.5. Corrosion products were occasionally ruptured on the steel surface after 4 and 7 days of exposure (Figure 20). Beneath such damaged layers, localized corrosion was observed after removal of corrosion products. A thick and fragile layer of Fe_3C, in comparison to the baseline experiment (see Figure 12), was more vulnerable to rupture before $FeCO_3$ could precipitate within its pores and confer more mechanical support. Figure 17 shows a top and cross-section view of such damage in corrosion products possibly caused by fluid flow.

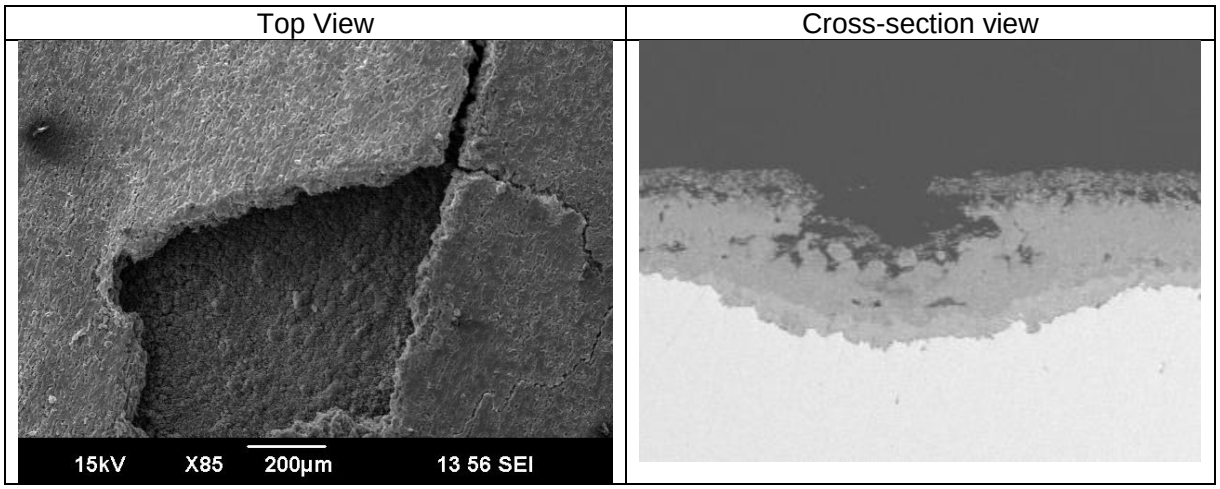

Figure 17: SEM images (top and cross section view) of ruptured corrosion products observed on specimens exposed to $MgCO_3$-satuarted solution with 4,200 ppm Mg^{2+} at 80°C, pCO_2 0.53 bar, 0.5 m/s, pH 5.5, ionic strength 0.6M, 1 wt.% NaCl

Figure 18 shows profilometry of specimens after removal of corrosion products by Clarke solution.[19] Localized corrosion was observed at locations where the corrosion product layer was damaged. The number of localized attack sites was limited, and the fractures were relatively wide. That is why the pitting ratio (maximum penetration rate over uniform corrosion rate) of such attacks is small. This observation of localized corrosion was repeatable in the presence of high concentration of Mg^{2+}. Table 3 provides more information regarding maximum pit depth and pitting ratio for two different experimental conditions where specimens where exposed to $MgCO_3$-saturated solution with 4,200 ppm Mg^{2+}. The maximum pitting ratio being lower than 2, this corrosion attack does not qualify as "pitting corrosion".

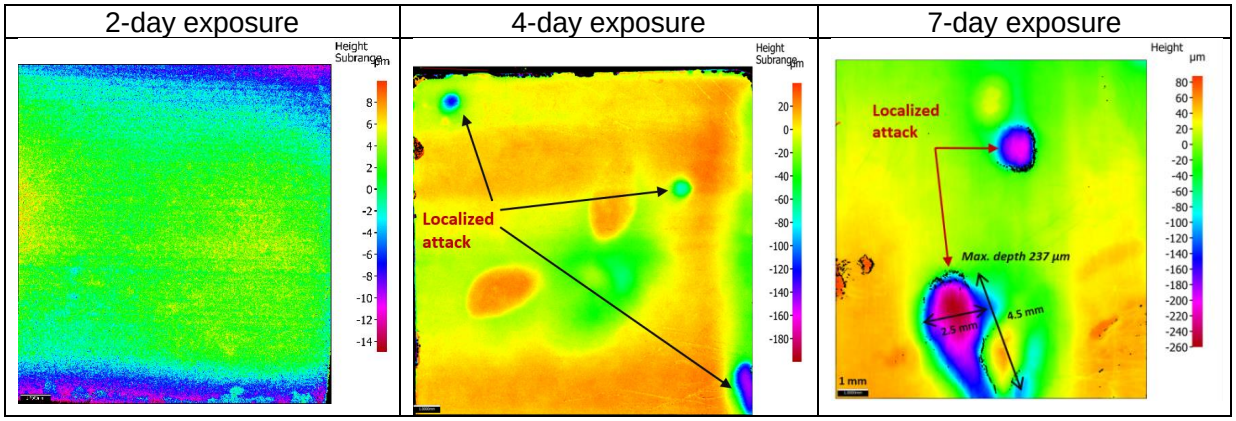

Figure 18: Profilometry of specimens after removing of corrosion product layers ($MgCO_3$-satuarted solution with 4,200 ppm Mg^{2+} at 80°C, pCO_2 0.53 bar, 0.5 m/s, pH 5.5, ionic strength 0.6M, 1wt% NaCl)

Table 3

Evolution of localized attacks on specimens exposed to 4,200 ppm Mg^{2+} at pH 5.5

Repeatability of localized corrosion in presence of high [Mg^{2+}] at pH 5.5	Experiment #A			
	Exposure time (day)	**Max pit (µm)**	**Max penetration rate (mm/y)**	**Pitting ratio**
	2	8	1.46	0.12
	4	140	12.78	1.08
	7	237	12.36	1.49
	Experiment #B (repeat of A)			
	Exposure time day	**Max pit (µm)**	**Max penetration rate (mm/y)**	**Pitting ratio**
	2	12	2.19	0.17
	4	200	16.22	1.59
	7	216	11.26	1.56

Based on the experimental results, a mechanism for the localized corrosion of mild steel exposed to high concentration of Mg^{2+} is proposed as illustrated in Figure **19**:

1) 1018 carbon steel is exposed to solution saturated with $MgCO_3$ and CO_2 with bulk pH 5.5.
2) Fe oxidatively dissolves and Fe^{2+} is released into solution. Consequently, a porous Fe_3C network is left behind on the steel surface and is growing, as a residue, over time. It is postulated that the presence of Mg^{2+} has hindered nucleation/growth of $FeCO_3$ crystals within Fe_3C pores. Therefore, corrosion rate is higher compared to Ca^{2+}-containing experiments at this stage of the corrosion process. Other researchers have also reported the inhibition effect of Mg^{2+} on carbonate nucleation in different aqueous systems.[3,20]
3) The fragile Fe_3C layer reach a critical thickness. Occasional breakage occurs possibly due to internal stress within the Fe_3C network as well as to flow effects.
4) Continuation of corrosion and Fe_3C development.
5) Achievement of favorable water chemistry for nucleation/precipitation of $FeCO_3$ within Fe_3C pores. At this stage, the very favorable water chemistry for precipitation of $FeCO_3$ overcomes the inhibiting effect of Mg^{2+} on $FeCO_3$ precipitation and as a result the general corrosion rate decreased.
6) Occurrence of localized corrosion where the steel is not covered with $FeCO_3$ (locations with damaged Fe_3C).
7) Retardation of localized corrosion rate due to further precipitation of $FeCO_3$.
8) Further development of $FeCO_3$ (inner layer) and $Fe_xMg_yCO_3$, x>>y (outer layer)

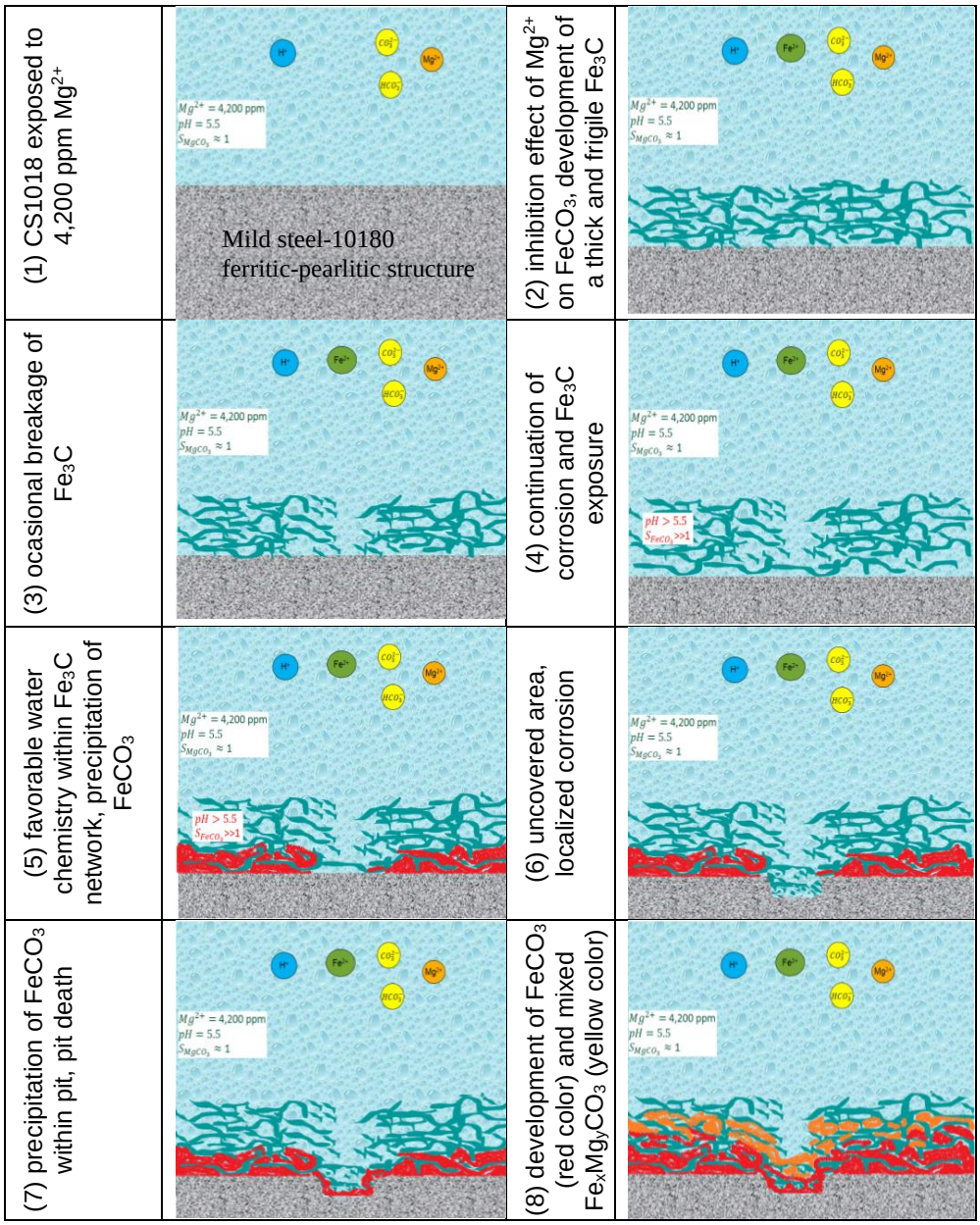

Figure 19: Proposed mechanism for the localized corrosion observed in presence of high [Mg^{2+}] for mild steel at 4,200 ppm Mg^{2+}, 80°C, pCO_2 0.53 bar, 0.5 m/s, pH 5.5, ionic strength 0.6M, 1 wt.% NaCl

Scenario 2: Effect of the Simultaneous Presence of Mg^{2+} and Ca^{2+} on CO_2 Corrosion at pH 5.5 (Test Condition Presented in Table 2)

In the previous section, the effect of Mg^{2+} and Ca^{2+} was studied separately. However, Mg^{2+} and Ca^{2+} are simultaneously observed in oilfield brines and it is consequently relevant to study the effect of these ions concurrently. In the current experimental scenario, the solution was

saturated with $CaCO_3$ (Ca^{2+} concentration *ca.* 6000 ppm) with addition of *ca.* 857 ppm Mg^{2+} as $MgCl_2$ salt (rendering a mass ratio of 7, Ca^{2+}/Mg^{2+}) based on conditions described in Table 2.
The trend of LPR corrosion rate over time with different water chemistry at pH 5.5 is presented in Figure 20. The presence of Mg^{2+} in a solution saturated with $CaCO_3$ (yellow line) seems to increase the general corrosion rate (compared to Ca^{2+}-containing solution without Mg^{2+}, dark blue line). Cumulative corrosion rate at day 2, 4 and 7 exposure times to different solutions obtained by WL method is provided in Figure 20. WL results, which agree with the LPR data, show that corrosion in the presence of 4,200 ppm Mg^{2+} is higher than the other scenarios at each measuring point. The addition of 857 ppm Mg^{2+} to a $CaCO_3$-saturated solution (yellow line) clearly increases the corrosion rate compared to a $CaCO_3$-saturated solution with no Mg^{2+} (dark blue line).

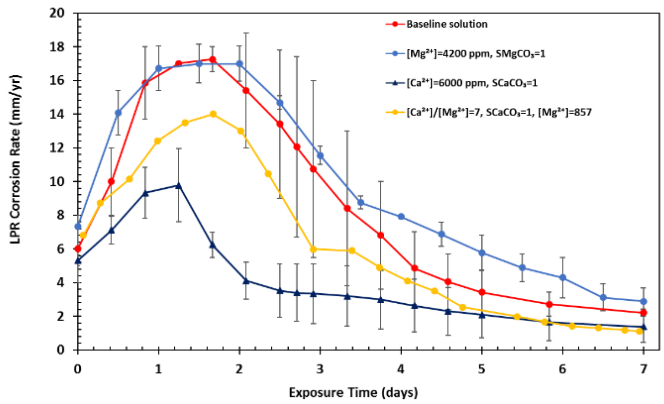

Figure 20: Trend of corrosion rate obtained by LPR over time at 80°C, pCO_2 0.53 bar, 0.5 m/s, pH 5.5, ionic strength 0.6M [baseline (red), 6000 ppm Ca^{2+} (dark blue), Ca^{2+}/Mg^{2+}=7 (yellow), and 4200 ppm Mg^{2+} (light blue)]

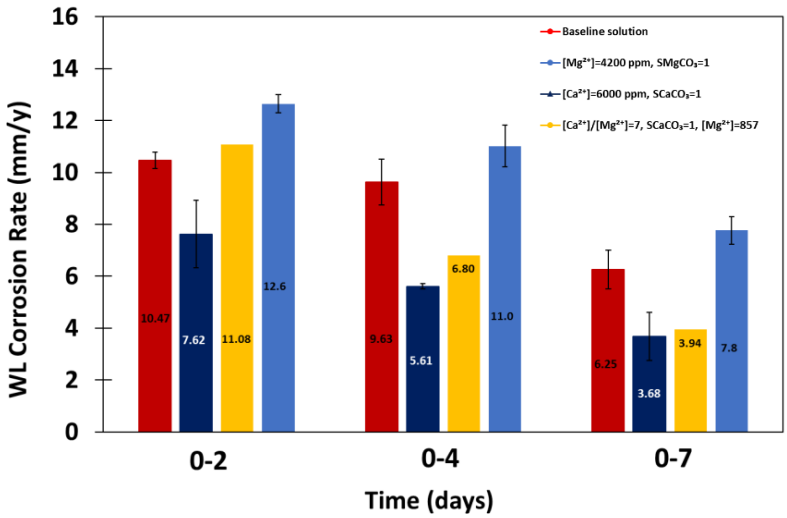

Figure 21: Cumulative corrosion rate obtained by WL over time at 80°C, pCO_2 0.53 bar, 0.5 m/s, pH 5.5, ionic strength 0.6M [baseline (red), 6000 ppm Ca^{2+} (dark blue), Ca^{2+}/Mg^{2+}=7 (yellow), and 4200 ppm Mg^{2+} (light blue)]

SEM and EDS analysis revealed that a lesser quantity of carbonates precipitated on top of the Fe_3C layers with the simultaneous presence of Mg^{2+} and Ca^{2+}, compared to a solution solely saturated with $CaCO_3$. It seems that the presence of Mg^{2+} diminished precipitation of carbonate crystals. Figure 22 illustrates SEM/EDS data, for comparison, for two solutions: (a) Ca^{2+}/Mg^{2+}=7, S_{CaCO3}=1 and (b) Ca^{2+}= 6000 ppm, S_{CaCO3}=1.

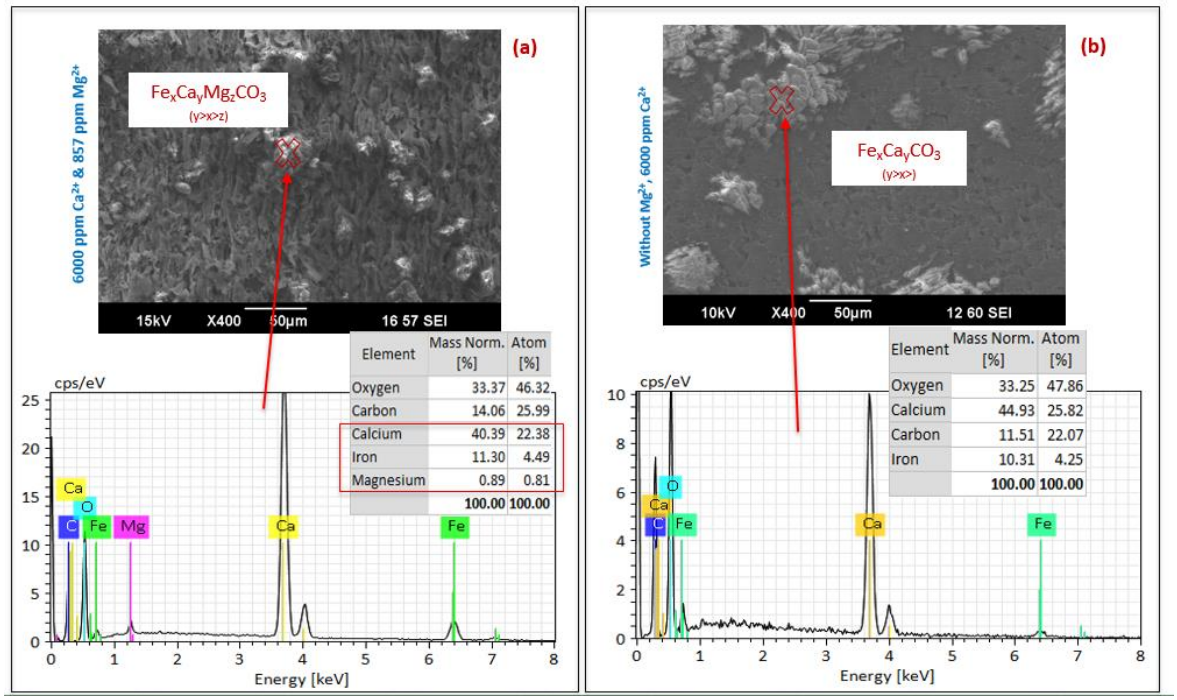

Figure 22: Comparison of SEM/EDS results for two solutions at 80°C, pCO_2 0.53 bar, 0.5 m/s, pH 5.5, ionic strength 0.68 M [**(a)**; Ca^{2+}/Mg^{2+}=7, $SCaCO_3$=1 & **(b)** Ca^{2+}= 6000 ppm, S_{CaCO3}=1(ref. [12])]

Figure 23 shows EDS line scan analysis of a cross-sectioned specimen after 7 days of exposure to the solution saturated with $CaCO_3$ and in the presence of 857 ppm Mg^{2+}. This analysis revealed that a mixed solid solution of $Fe_xCa_yMg_zCO_3$ (x>y, z is trace) is formed at the outer layer whereas the inner layer was a pure $FeCO_3$ phase.

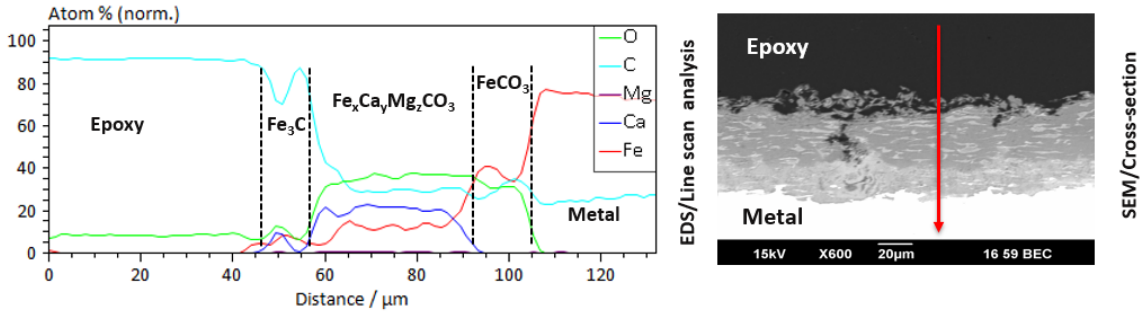

Figure 23: EDS line scan analysis of the surface layers developed on a specimen after 7 days of exposure to a $CaCO_3$-saturated electrolyte with 857 ppm Mg^{2+} at 80°C, pCO_2 0.53 bar, 0.5 m/s, pH 5.5, ionic strength 0.6M

CONCLUSIONS

The following conclusions can be drawn:

- Localized corrosion was observed in the presence of a high concentration of Mg^{2+}. A descriptive model is provided for this finding.
- The presence of low and high concentrations of Ca^{2+} (at pH 6.2 and 5.5, respectively), as far as solution is under saturated or saturated with respect to $CaCO_3$, would not endanger protectiveness of corrosion products and no localized corrosion was observed.[11, 13]
- A uniformly formed $CaCO_3$ scale on the steel surface is not protective, however, its presence facilitates the formation of protective $FeCO_3$ as the inner-layer corrosion product. Partial precipitation of $CaCO_3$ on the substrate might lead to localized corrosion.[12]
- No localized corrosion was observed for electrolytes with a simultaneous presence of Ca^{2+} and Mg^{2+}.
- The presence of Mg^{2+} adversely influenced precipitation of carbonates ($FeCO_3$ and $CaCO_3$) at the outer layer in solutions saturated with respect to $CaCO_3$.

ACKNOWLEDGMENTS

The author would like to thank the following companies for their financial support: Anadarko, Baker Hughes, BP, Chevron, Clariant Corporation, CNOOC, ConocoPhillips, DNV GL, ExxonMobil, M-I SWACO (Schlumberger), Multi-Chem (Halliburton), Occidental Oil Company, PTT, Saudi Aramco, SINOPEC (China Petroleum) and TOTAL.

REFERENCES

[1] Z. Dai, A. Kan, F. Zhang, and M. Tomson, "A Thermodynamic Model for the Solubility Prediction of Barite, Calcite, Gypsum, and Anhydrite, and the Association Constant

Estimation of $CaSO_4$ Ion Pair up to 250 °C and 22000 psi," *J. Chem. Eng. Data*, vol. 60, no. 3, pp. 766–774, 2015.
[2] D. H. Case, F. Wang, and D. E. Giammar, "Precipitation of Magnesium Carbonates as a Function of Temperature, Solution Composition, and Presence of a Silicate Mineral Substrate," *Environ. Eng. Sci.*, vol. 28, no. 12, pp. 881–889, 2011.
[3] M. Hänchen, V. Prigiobbe, R. Baciocchi, and M. Mazzotti, "Precipitation in the Mg-carbonate system—effects of temperature and CO_2 pressure," *Chem. Eng. Sci.*, vol. 63, no. 4, pp. 1012–1028, 2008.
[4] Z. D. Cui, S. L. Wu, S. L. Zhu, and X. J. Yang, "Study on corrosion properties of pipelines in simulated produced water saturated with supercritical CO_2," *Appl. Surf. Sci.*, vol. 252, no. 6, pp. 2368–2374, 2006.
[5] C. de Waard, U. Lotz, and D. E. Milliams, "Predictive Model for CO_2 Corrosion Engineering in Wet Natural Gas Pipelines," *Corrosion*, vol. 47, no. 12, pp. 976–985, 1991.
[6] K. Gao, F. Yu, X. Pang, and G. Zhang, "Mechanical Properties of CO_2 Corrosion Product Scales and Their Relationship to Corrosion Rates," *Corros. Sci.*, vol. 50, no. 10, pp. 2796–2803, 2008.
[7] B. R. Linter and G. T. Burstein, "Reactions of pipeline steels in carbon dioxide solutions," *Corros. Sci.*, vol. 41, no. 1, pp. 117–139, 1999.
[8] J. Han, J. W. Carey, and J. Zhang, "Effect of sodium chloride on corrosion of mild steel in CO_2-saturated brines," *J. Appl. Electrochem.*, vol. 41, no. 6, pp. 741–749, 2011.
[9] P. E. Dresel and A. W. Rose, "Chemistry and Origin of Oil and Gas Well Brines in Western Pennsylvania," The Pennsylvania State University, Open-File Report OFOG 10–01.0, 2010.
[10] H. Mansoori, D. Young, B. Brown, and M. Singer, "Influence of Calcium and Magnesium Ions on CO_2 Corrosion of Carbon Steel in Oil and Gas Production Systems-A Review," *J. Nat. Gas Sci. Eng.*, vol. 59, pp. 287–296, 2018.
[11] H. Mansoori, D. Young, B. Brown, S. Nesic, and M. Singer, "Effect of $CaCO_3$-Saturated Solution on CO_2 Corrosion of Mild Steel Explored in a System with Controlled Water Chemistry and Well-Defined Mass Transfer Conditions," *Corros. Sci.*, vol. 158, pp. 108078 2019.
[12] H. Mansoori, D. Young, B. Brown, S. Nesic, and M. Singer, "Effect of Calcium Ions and $CaCO_3$ Scale on the CO_2 Corrosion Mechanism of Mild Steel," in *NACE International*, Paper No. 13000, 2019.
[13] H. Mansoori, D. Young, B. Brown, S. Nesic, and M. Singer, "CO_2 Corrosion of Mild Steel Exposed to $CaCO_3$-Saturated Aqueous Solutions," *Corrosion*, vol. 75, no. 11, pp. 1281-1284, 2019.
[14] S. N. Esmaeely, D. Young, B. Brown, and S. Nesic, "Effect of Incorporation of Calcium into Iron Carbonate Protective Layers in CO_2 Corrosion of Mild Steel," *Corrosion*, vol. 73, no. 3, pp. 238–246, 2016.
[15] X. Zhong, B. Brown, W. Li, S. Nesic, and M. Singer, "How to Maintain a Stable Solution Chemistry when Simulating CO_2 Corrosion in a Small Volume Laboratory System," in *NACE International*, Paper No. 7780, 2016.
[16] Y. Yang, B. Brown, M. E. Gennaro, and B. Molinas, "Mechanical Strength and Removal of a Protective Iron Carbonate Layer Formed on Mild Steel in CO_2 Corrosion," in *NACE International*, Paper No. 10383, 2010.
[17] F. Madani Sani, B. Brown, Z. Belarbi, and S. Nesic, "An Experimental Investigation on the Effect of Salt Concentration on Uniform CO2 Corrosion," in *NACE International*, Paper No.13026, 2019.
[18] F. Farelas, M. Galicia, B. Brown, S. Nesic, and H. Castaneda, "Evolution of dissolution processes at the interface of carbon steel corroding in a CO_2 environment studied by EIS," *Corros. Sci.*, vol. 52, no. 2, pp. 509–517, 2010.

[19] ASTM G1, “Standard Practice for Preparing, Cleaning, and Evaluating Corrosion Test.” ASTM International, 2011.
[20] S.H. Lin and S. C. Dexter, “Effects of Temperature and Magnesium Ions on Calcareous Deposition,” *Corrosion*, vol. 44, no. 9, pp. 615–622,1988.